

# Prediction of fine scale jet mixing noise refraction effects using a two-step propagation technique

Yann Martelet  
Airbus, Toulouse, France

Christophe Bailly  
Laboratoire de Mécanique des Fluides et d'Acoustique, Ecole Centrale de Lyon, Ecully, France

## Summary

A noise prediction method for fine scale jet mixing noise based on Tam and Auriault's methodology [1] using a two-step propagation technique is developed. The core of this study is to split the path of the sound wave in two parts using geometrical acoustics in order to separate the propagation in the jet and the propagation through the external medium. A Green function for the pressure taking into account refraction effects is introduced. The aeroacoustic sources will be modelled thanks to a statistical approach, and are numerically computed from a Reynolds-Averaged Navier-Stokes computation.

PACS no. 43.28.-g, 43.28.+h

## 1. Introduction

Jet mixing noise has been lengthly studied and comprehensive models have been proposed by Tam and Auriault [1], Morris and Boluriaan [2] and more recently by Miller [3]. The request for more accurate predictions and the changes in turbofan-engine geometry have revived the interest in this topic. The jet mixing noise is the noise generated by the turbulent structures located in the mixing layer between the jet and the possible external flow. As described by Tam and Golebiowski [4], the fine scale and the large scale turbulence contribute to jet noise. The fine scale turbulence generates noise which dominates the jet mixing noise spectrum upstream and at a polar angle of  $90^\circ$  whereas the noise associated with the large scale turbulence dominates the spectrum downstream. The jet mixing noise could be computed using direct acoustic predictions using scale resolving simulations such as direct numerical simulation, large eddy simulation or detached eddy simulation [5] coupled with high accuracy propagators but these solutions are still difficult to apply on complex geometries. A statistical approach is often preferred to calculate aeroacoustic sources using the turbulence data provided by a Reynolds-Averaged Navier-Stokes (RANS) computation. This method is especially useful in an

industrial context because of the reasonable restitution time needed for the fluid dynamics computation. Therefore, a design loop can quickly be created in order to evaluate the effect of a geometrical change on the produced noise. The aim of this study is to present a methodology based on Tam and Auriault's model for predicting the jet mixing noise induced by fine scale turbulence and the directivity including the refraction through the mixing layer and the presence of a cone of silence near the jet axis. The acoustic propagation is done by parts in the framework of the geometrical acoustic. The first part is through the jet, from the sources to the point where the refraction will take place and then to the observer. The use of ray tracing for the propagation is done in order to anticipate future problematics such as more complex geometries involved in installed configurations. First, source modelisation and the obtention of the noise spectrum formula following Tam and Auriault's work will be detailed. Then, the two-step propagation technique will be presented as well as the equations used for the localisation of the refraction point. Finally, noise predictions will be shown and compared to a realistic isolated configuration case (EXEJET) [6] at the sideline operating point.

## 2. Expression of the noise spectrum

### 2.1. Turbulence inputs

The sources are modelled with data provided by a RANS computation. The intensity is computed using as the source term the Boussinesq eddy viscosity model for the Reynolds stresses

$$-\overline{\rho u_i u_j} = 2\mu_t \left( S_{ij} - \frac{1}{3} S_{kk} \delta_{ij} \right) - \frac{2}{3} \bar{\rho} k_s \delta_{ij} \quad (1)$$

$$S_{ij} = \left( \frac{\partial \bar{u}_i}{\partial x_j} + \frac{\partial \bar{u}_j}{\partial x_i} \right) \quad (2)$$

where  $\bar{u}$  and  $u$  are respectively the mean and fluctuating velocity,  $\bar{\rho}$  is the mean density,  $\mu_t$  is the turbulent viscosity.

This source term is then arbitrarily simplified to only consider the source term

$$q_s = \frac{2}{3} \bar{\rho} k_s \quad (3)$$

where  $k_s$  is the turbulent kinetic energy, assumed to be associated with the fine scale structures.

Tam and Auriault [1] argue that using this formulation would only describe the noise generated by the fine scale turbulence. Because of the nature of the source used, it would not describe on a physical point of view, the noise production mechanism of the large scale turbulence. In future works, a source term  $q = q_s + q_l$  could be used in order to take into account both contributions.

For the noise prediction using Tam and Auriault's model, the explicit expression of the source term  $q_s$  is not directly needed but the two-point time-space correlation of the axial velocity is. That yields [7]

$$\left\langle \frac{Dq_s(\vec{x}_{S_1}, t_1)}{Dt_1} \frac{Dq_s(\vec{x}_{S_2}, t_2)}{Dt_2} \right\rangle = \frac{\hat{q}_s^2}{c_{jet}^2 \tau_s^2} \times \exp \left( -\frac{|\xi|}{\bar{u} \tau_s} - \ln 2 \left[ \frac{[\xi - \bar{u} \tau]^2}{l_s^2} + \frac{\eta^2}{l_s^2} + \frac{\zeta^2}{l_s^2} \right] \right) \quad (4)$$

with  $\xi = x_1 - x_2$ ,  $\eta = y_1 - y_2$ ,  $\zeta = z_1 - z_2$  and  $\tau = t_1 - t_2$ .

A few terms need to be explicitated: the characteristic decay time  $\tau_s = c_\tau k_s / \epsilon$ , the characteristic length scale in the moving frame of the mean flow  $l_s = c_l k_s^{3/2} / \epsilon$ , and the intensity of the fluctuation of the kinetic energy of the fine scale turbulence  $\hat{q}_s = A^2 q_s^2 c_{jet}^2$ . These 3 variables are directly calculated with the turbulence data provided by the RANS simulation. Finally,  $\bar{u}$  is the mean local velocity,  $c_{jet}$  is the local sound speed. Additionally,  $A$ ,  $c_l$  and  $c_\tau$  are fitted constants. The values of these constants are taken from Tam and Auriault [1].

### 2.2. Tam and Auriault's formulation

Tam and Auriault sets the problem using the Reynolds-Averaged Navier-Stokes equations. They are linearized and simplified using the approximation of axisymmetric and locally parallel mean flow.

The problem is solved by first introducing the Green function and the the adjoint problem. After tedious calculations that are not presented here but are detailed in Tam and Auriault's paper a link between the pressure at a point  $M$  and the adjoint pressure is obtained

$$p(\vec{x}_M, t) = \iiint_{-\infty}^{\infty} \frac{Dq_s}{Dt_1} p_a(\vec{x}_S, \vec{x}_M, \omega) \times e^{-i\omega(t-t_1)} d\omega d\vec{x}_S dt_1 \quad (5)$$

The formula for the noise spectrum at a point  $M$  and a frequency  $\omega$  is given by

$$S(\vec{x}_M, \omega) = \frac{1}{2\pi} \int_{-\infty}^{\infty} \langle p(\vec{x}_M, t_1) p(\vec{x}_M, t_1 + \tau) \rangle \times e^{i\omega\tau} d\tau \quad (6)$$

By combining both equations and introducing the modelisation of the sources using the two-point time-space correlation of the axial velocity expressed in the previous section, the noise spectrum can be computed.

After tedious calculations, the following formula is obtained for the noise spectrum

$$S(\vec{x}_M, \omega) = 4\pi \left( \frac{\pi}{\ln 2} \right)^{3/2} \iiint_{-\infty}^{\infty} |p_a(\vec{x}_S, \vec{x}_M; \omega)|^2 I_s d\vec{x}_S \quad (7)$$

where the source part is

$$I_s = \frac{\hat{q}_s^2 l_s^3}{c^2 \tau_s} \frac{\exp \left[ -\frac{\omega^2 l_s^2}{4 \ln 2 \bar{u}^2} \right]}{1 + \left( 1 - \frac{\bar{u}}{c_{ext}} \cos \theta \right)^2 \omega^2 \tau_s^2} \quad (8)$$

and  $c_{ext}$  is the ambient speed of sound

Using Eq (7), the global process for the noise prediction can be highlighted. The noise spectrum is the integration over the source volume of the multiplication of two terms, a propagation term with  $p_a$  and a source term with  $I_s$ . The first step is to compute the source term for each point in the mixing layer. Then, the propagation term is computed as explained in the following sections. Finally, all the contributions in the discretized source domain are summed using a second order integration on the cells of the mesh to obtain the jet mixing noise predictions.

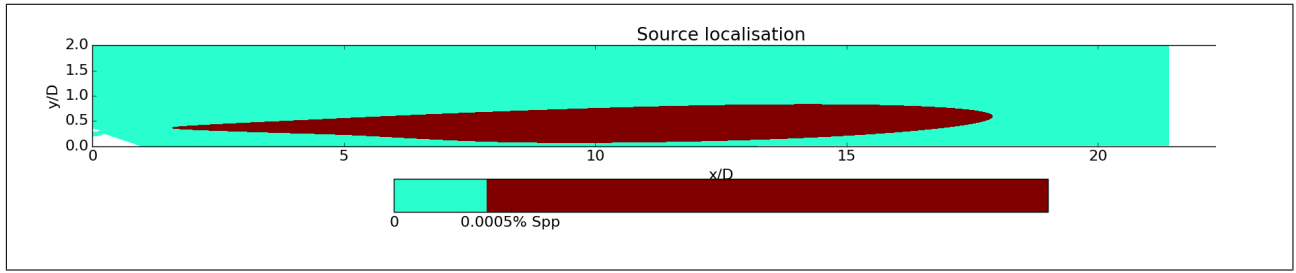


Figure 1. Representation of the intensity the source term  $I_s$  at a frequency  $f = 100Hz$

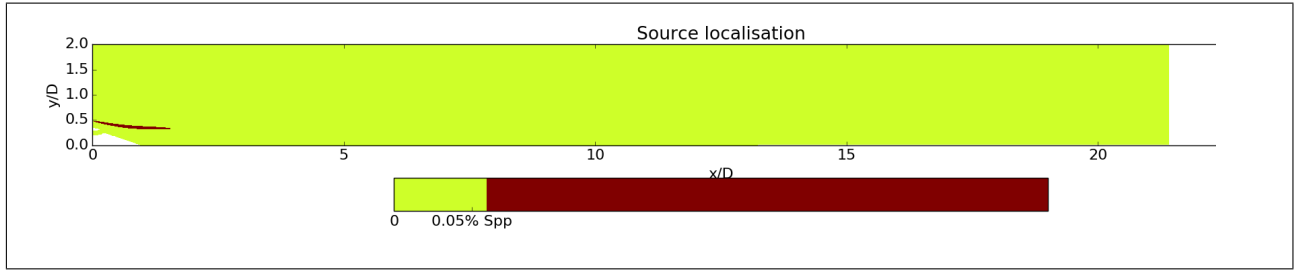


Figure 2. Representation of the intensity source term  $I_s$  at a frequency  $f = 10kHz$

### 2.3. Frequency dependency

By examining the source term  $I_s$ , a frequency dependency can be found and by plotting it for different frequencies, a link between the position in the jet, and in a way the length scale, and the source intensity can be shown. The reader may refer to Figure 1 for the source field at 100Hz and Figure 2 for the source field at 10kHz. Note that only one slice of the axisymmetrical flow is plotted. For high frequencies the source domain is small, intense and located right at the nozzle exit whereas for lower frequencies, the source domain is larger, more spread and located more downstream. It can be deduced that according to this modelisation, among the fine-scale vortices, the smaller ones which are located right at the nozzle exit would be responsible for high frequency noise. When travelling downstream these vortices will gain in size and would then emit noise at lower frequencies.

## 3. Propagation

### 3.1. Ray Theory

As announced in the introduction, the propagation will be done using the ray theory. This theory is explained in details in numerous articles like in Candel [8]. For one ray going from S to M passing by R where the refraction happens, as illustrated in Figure 3, the pressure in M is

$$p(\vec{x}_M, \omega) = p(\vec{x}_{R^-}, \vec{x}_S, \omega) K_D K_T \times \Phi_{ext}(\vec{x}_M, \vec{x}_{R^+}, \omega) \quad (9)$$

$$\Phi_{ext} = e^{ik' [|\vec{x}_M - \vec{x}_{R^+}| + M_{ext}(x'_M - x'_{R^+})]} \quad (10)$$

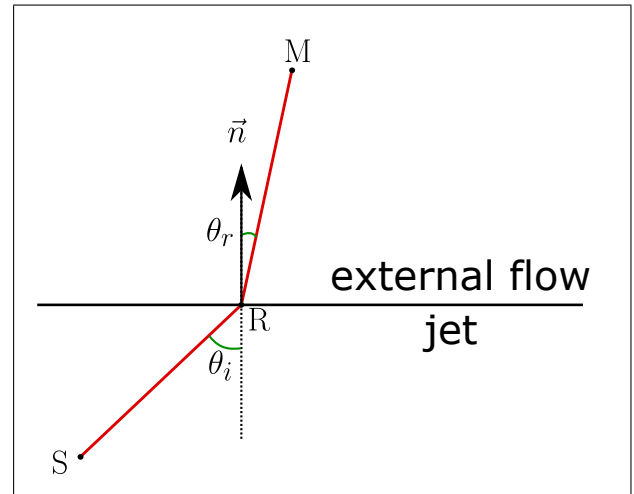


Figure 3. Illustration of a ray going from the source point S to the observer M through the refraction point R, illustrating the refraction angles

$$p(\vec{x}_{R^-}, \vec{x}_S, \omega) = I_s T(\vec{x}_{R^-}, \vec{x}_S, \omega) \quad (11)$$

$$T(\vec{x}_{R^-}, \vec{x}_S, \omega) = \frac{-e^{ik' [|\vec{x}_{R^-} - \vec{x}_S| + M_{jet}(x'_{R^-} - x'_S)]}}{4\pi \sqrt{1 - M_{jet}^2} |\vec{x}_{R^-} - \vec{x}_S|} \quad (12)$$

where this change of variable dependent on the Mach number of the corresponding medium

$$x = \sqrt{1 - M^2} x' \quad (13)$$

$$y = y' \quad (14)$$

$$z = z' \quad (15)$$

$$k = \sqrt{1 - M^2} k' \quad (16)$$

with  $k = 2\pi/\lambda$  the wavenumber.  $K_D$  is the divergence coefficient and  $K_T$  is the transmission coefficient.

The classical criteria for the application of the ray theory is  $R \gg \lambda$  with  $\lambda$  the wavelength and  $R$  being the the maximum radius curvature of the reflection surface. Nevertheless, years of work with such techniques at Airbus have shown that even if it seems surprising for the lower part of the frequency range, the results using ray techniques still holds until  $kR > 2$ .

Lastly, two coefficients have to be introduced in order to properly take into account all the effects involved into the refraction phenomenon. The first one is the transmission factor  $K_T$  describing the change in intensity upon switching medium. The second one is the divergence coefficient  $K_D$  describing the reduction of intensity following the passage through a curved interface. Both factors are applied on the pressure.

### 3.2. Transmission coefficient

Because of the difference in the inherent characteristics of both media, the pressure field generated by a same source in the jet or in the external flow will be different. This has been already well explained in the litterature by Morse and Ingard [9] for example. The transmission factor  $K_T$  is given in their book

$$K_T = \frac{2\rho_{ext}c_{ext}^2 \cos(2\theta_i)}{\rho_{ext}c_{ext}^2 \cos(2\theta_i) + \rho_{jet}c_{jet}^2 \cos(2\theta_e)} \quad (17)$$

with the refraction angles  $\theta_i$  and  $\theta_r$  taken as shown in Figure 3.

### 3.3. Divergence coefficient

When propagating in a homogeneous medium, a pencil ray keeps a constant section but when passing through a curved surface, the section will evolve depending on the curvature of the interface but also on the characteristics of both medium through the reflection angles. This has been described by Deschamps [10], explaining how to obtain the principal radii of curvature,  $r_1^e$  and  $r_2^e$ , of the wavefront after refraction. With the curvatures, the divergence coefficient can be expressed as

$$K_D = \sqrt{\frac{r_1^e r_2^e}{(r_1^e + \|\vec{RM}\|)(r_2^e + \|\vec{RM}\|)}} \quad (18)$$

### 3.4. Integration of the ray theory in the Tam and Auriault model [1]

The system of equations used as a starting point by Tam and Auriault can be simplified for the case of an uniform mean flow approximation and therefore reduced to the inhomogeneous convected Helmholtz equation

$$\frac{1}{c_{ext}^2} \frac{D^2 p}{Dt^2} - \nabla^2 p = \nabla^2 q_s \quad (19)$$

This equation can be solved in the Fourier domain using the convected Green function in free space  $G$  defined by

$$\frac{1}{c_{ext}^2} \frac{D^2 G}{Dt^2} - \nabla^2 G = \delta(\vec{x} - \vec{x}_1) \quad (20)$$

This gives

$$p(\vec{x}, t) = \iiint_{-\infty}^{\infty} G(\vec{x}, \vec{x}_1, \omega) \nabla_1^2 \times q_s e^{-i\omega(t-t_1)} d\omega d\vec{x}_1 dt_1 \quad (21)$$

By introducing the adjoint problem and some integrations by parts, it can be shown that the pressure field can be expressed as

$$p(\vec{x}, t) = \frac{-1}{c_{ext}^2} \iiint_{-\infty}^{\infty} \frac{D}{Dt_1} G(\vec{x}, \vec{x}_1, \omega) \times \frac{Dq_s}{Dt_1} e^{-i\omega(t-t_1)} d\omega d\vec{x}_1 dt_1 \quad (22)$$

where the subscript  $_1$  indicates a derivation with respect to  $\vec{x}_1$ .

By linking this relationship (22) to Eq (5) it is found by identification that

$$p_a(\vec{x}_1, \vec{x}, \omega) = \frac{1}{c_{ext}^2} \frac{D}{Dt_1} G(\vec{x}, \vec{x}_1, \omega) \quad (23)$$

If a dimensional analysis is done on Eq (21) and Eq (9) the following terms can be linked

$$I_s \sim \nabla_1^2 q_s \quad (24)$$

$$G(\vec{x}, \vec{x}_1, \omega) \sim TK_D K_T \Phi_{ext}$$

Therefore, in the case of a source domain and not just a single ray, one has

$$p(\vec{x}_M, t) = \iiint_{-\infty}^{\infty} T \nabla_1^2 q_s e^{-i\omega(t-t_1)} \times K_D K_T \Phi_{ext} d\omega d\vec{x}_1 dt_1 \quad (25)$$

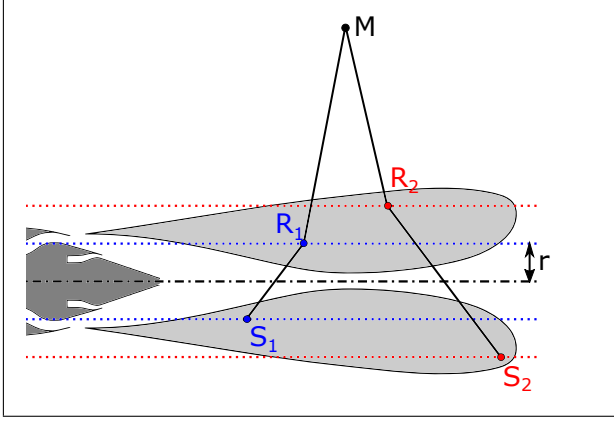


Figure 4. Application of the cylinder modelisation on a realistic source domain for two sources  $S_1$  and  $S_2$

Now a development analog as from Eq (21) to Eq (22) must be performed. For it to be done,  $K_D K_T \Phi_{ext}$  will be considered independent of  $x_S$ , which is not technically the case for  $K_T$  and  $K_D$ . Nevertheless, because this part of the formula handles the propagation from R to M this assumption is done. That leads to

$$p(x_M, t) = \int_{-\infty}^{\infty} \int \int \frac{DT Dq_s}{Dt_1 Dt_1} e^{-i\omega(t-t_1)} K_D K_T \Phi_{ext} d\omega d\vec{x}_1 dt_1 \quad (26)$$

By linking this expression to Eq (5) it is found that

$$p_a(\vec{x}_1, \vec{x}, \omega) = \left[ \frac{1}{c_{ext}^2} \frac{D}{Dt_1} T(\vec{x}_{R-}, \vec{x}_1, \omega) \right] \times K_D K_T \Phi_{ext} \quad (27)$$

This can be directly substituted in Eq (7).

### 3.5. Equations for the localisation of the refraction location

In this model, the jet will be seen as a cylinder oriented in the direction of  $\vec{x}$ , the downstream jet axis. Inside this cylinder is the first propagation medium, the jet, and outside is the second, the external flow. The mixing layer is therefore considered as infinitely thin. That means that all the sources are located on the cylinder surface and the refraction will happen also on the same cylinder.

In a more realistic configuration, the source domain is not a cylinder but a volume. Using only one radius for the source modelisation will induce the omission of a large portion of the sources. To fix this issue, the system of equation will be solved for a given number of coaxial cylinders so that all the sources of importance depending on the frequency are considered as explained above as shown in Figure 4. One of the drawback of this method is that the path in the jet

will be then smaller for source closer to the jet axis than for sources further away from the jet axis. Nevertheless, because the predictions are provided at the far field, this will not have that much of an influence on the quality of the final noise spectra.

The following equations will be used to build a system in order to find the position of the refraction point  $R$  using the coordinates of the observer  $M$  and the source point  $S$ . There are 5 unknown variables: the 3 coordinates of  $R$  and the two refraction angles so 5 equations are needed.

The refraction phenomenon occurs in a plan defined by  $S$ ,  $R$  and  $M$ . The following mixed product is then null:  $(\vec{RS} \times \vec{RM}) \cdot \vec{n} = 0$ , with  $\vec{n}$  the normal to the cylinder in  $R$

After calculation and with  $R$  expressed in cylindrical coordinates that leads to

$$\begin{aligned} \cos \theta_R (x_M z_S - z_M x_S + x_R (z_M - z_S)) + \\ \sin \theta_R (y_M x_S - x_M y_S + x_R (y_S - y_M)) = 0 \end{aligned} \quad (28)$$

Note that in the presence of an external flow,  $\vec{RS}$ ,  $\vec{RM}$  and  $\vec{n}$  are not coplanar anymore. The coordinates of  $M$  to be used are the one if the velocity of the external flow would be null. The propagation will nevertheless be done with the proper coordinates.

The source point  $S$  and the refraction point  $R$  are both on the same cylinder of radius  $r$ , as pictured in Figure 4, so it is straightforward that

$$r_R = r_S = r \quad (29)$$

The refraction angles are introduced using the scalar product of the incident ray  $\vec{SR}$  and of the emerging ray  $\vec{RM}$  with the normal vector  $\vec{n}$  to the cylinder surface.

$$\begin{aligned} \vec{RS} \cdot \vec{n} &= (y_S - y_R) \cos \theta_R \\ &+ (z_S - z_R) \sin \theta_R \\ &= \|\vec{RS}\| \cos \theta_i \end{aligned} \quad (30)$$

$$\begin{aligned} \vec{RM} \cdot \vec{n} &= (y_M - y_R) \cos \theta_R \\ &+ (z_M - z_R) \sin \theta_R \\ &= \|\vec{RM}\| \cos \theta_e \end{aligned} \quad (31)$$

Finally, the last equation is the Snell's law

$$U_{jet} X_t + \frac{c_{jet}}{\sin \theta_i} = \frac{c_{ext}}{\sin \theta_e} \quad (32)$$

The numerical resolution gives a map of the position of the refraction point as pictured in Figure 5. The red points represent the source locations and in blue are pictured the refraction location for an observer at a polar angle of  $90^\circ$ .

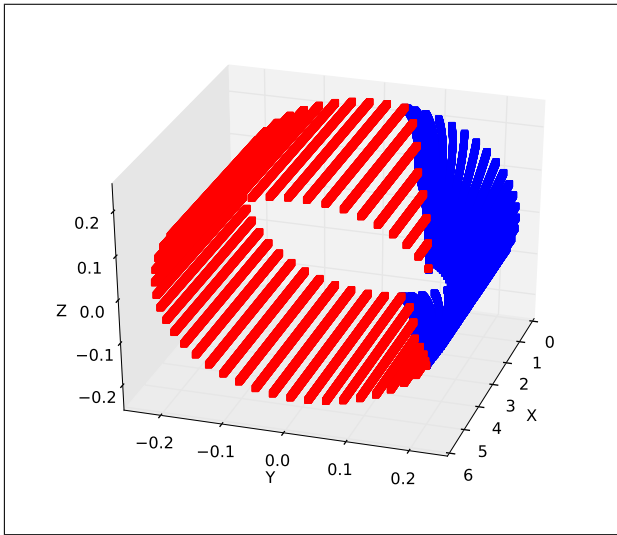


Figure 5. Representation of the sources (in red) and their corresponding refraction locations (in blue) for an observer located at  $90^\circ$

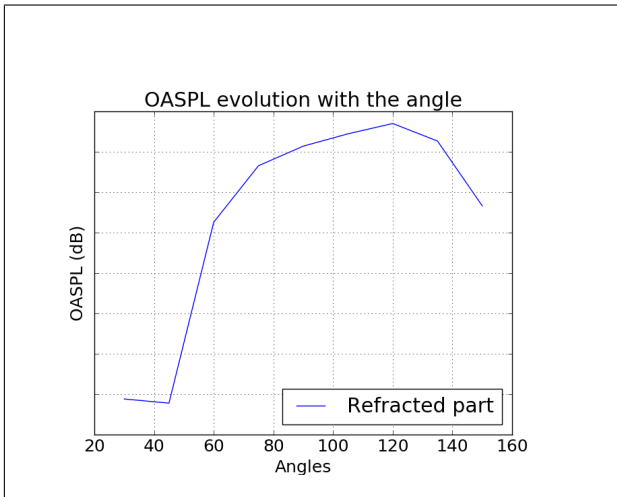


Figure 6. OASPL prediction for the refracted sources

#### 4. Results

In the following section, results of the jet mixing noise prediction will be presented and compared to the EXEJET test case. For this nozzle, the diameter of the core and the bypass are respectively 130mm and 220mm. The measurements and the prediction are both made for an isolated configuration at sideline condition with an external flow. That means  $M_{jet} = 0.78$  and  $M_{ext} = 0.23$ . As a side note, the jet is coaxial even though this is not taken into account in the model and with a temperature ratio  $T_{core}/T_{fan} = 2.43$ .

In a first time, the OASPL for the refracted part in Figure 6 and for the direct part in Figure 7 are compared in order to weigh each contribution on the total noise. First of all, by looking at the noise prediction for the refracted contribution, it can be observed

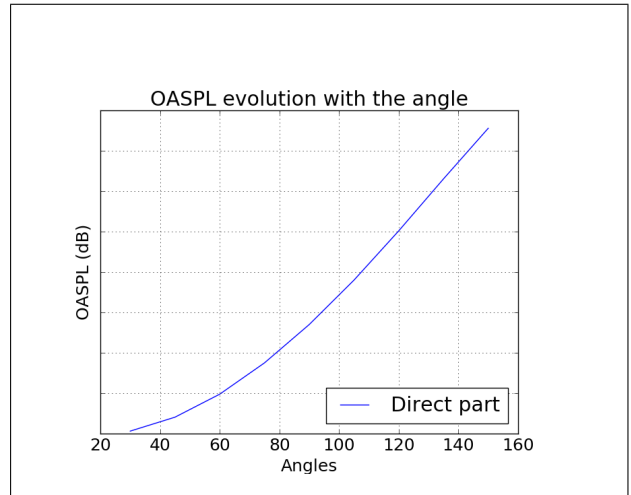


Figure 7. OASPL prediction for the direct sources

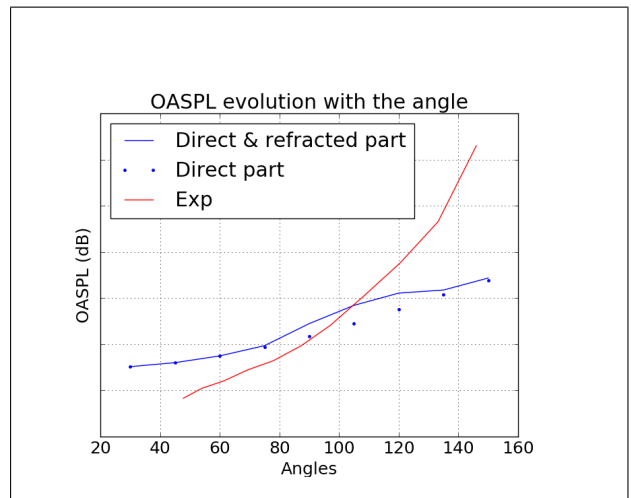


Figure 8. OASPL prediction for all the sources

that there is in fact a sharp reduction of noise when going further from the polar angle of  $120^\circ$ . The two reductions are due to the fact that for an observer way upstream or downstream, the incident angles of all the rays will be quite high thus leading to a greater attenuation by both the transmission factor and the divergence factor. The reason behind a maximum of energy at around  $120^\circ$  is because it corresponds to an observer at an axial position corresponding to the center of the useful jet domain, meaning the part of the jet where sources are present. Then, by comparing the noise level of the two contributions, it can be expected that the total noise level will be mainly driven by the direct sources with only an impact around  $120^\circ$ .

The OASPL of the total fine scale jet mixing noise is plotted in Figure 8. As expected the noise level is equal to the one from the direct part for an observer at a polar angle of  $30^\circ$  to  $75^\circ$  and above  $135^\circ$  with a bump from the refraction part around  $105^\circ$ . There is a constant augmentation of the noise level with the angle until  $120^\circ$  where it stops increasing and plateau

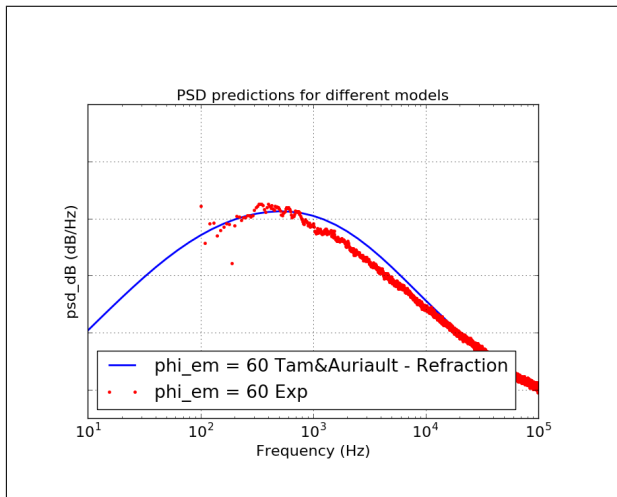


Figure 9. PSD prediction at a polar angle of 60°

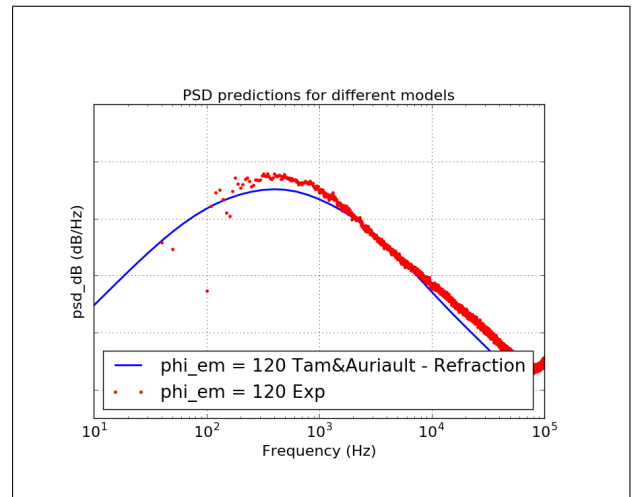


Figure 11. PSD prediction at a polar angle of 120°

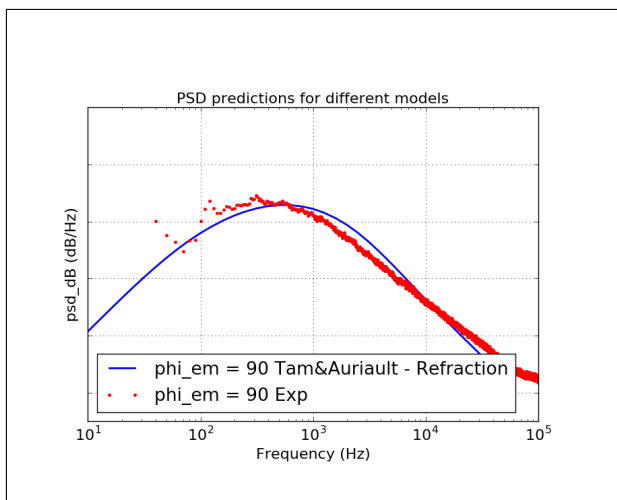


Figure 10. PSD prediction at a polar angle of 90°

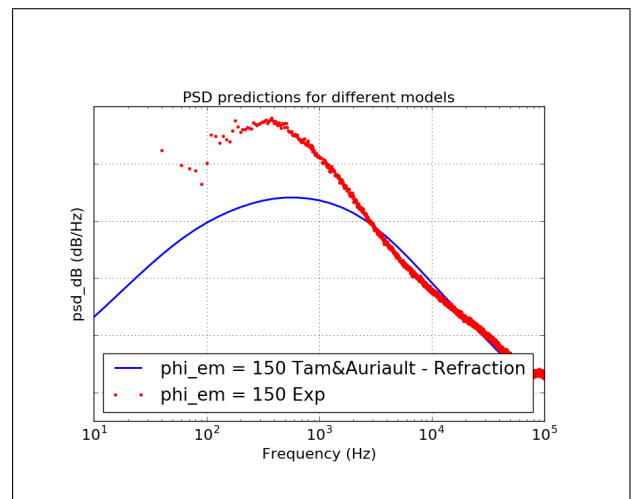


Figure 12. PSD prediction at a polar angle of 150°

until 150°. This is the cone of silence phenomenon as described by Tam et al. [4]

A few comments on the experimental data and more generally the frame of this study is required. The aforementioned cone of silence cannot be observed on the EXEJET measurements. This is due to the fact that downstream, the jet mixing noise is driven by a source that is currently not predicted by the model: the large scale turbulence. This is especially clear by looking at the PSD curves at a polar angle of 150° as presented in Figure 12. A secondary spectrum appears with a peak at a slightly lower frequency and a much higher amplitude. This source appears approximately at the same angle where the fine scale turbulence noise contribution plateau. Therefore, the noise level will not stagnate or reduce as expected but sharply increase. This aspect renders any absolute prediction of the noise level downstream impossible.

The next comparisons will be done using the PSD for the polar angles of 60° in Figure 9, 90° in Figure 10, 120° in Figure 11 and 150° in Figure 12. As a

reminder, no constant fit has been performed, the ones used in the present paper are those from Tam and Auriault [1]. The aim here is to observe the impact of the refraction on the evolution of the radiated noise compared to the experiment rather than optimizing the model for one particular test case.

The agreement with the experiment for polar angle below 90° is good in term of peak amplitude despite a slight frequency shift toward the high frequencies. This frequency shift increases with the polar angle too. The shape of the spectrum is slightly broader than the experiment and leads to a few overprediction in term of OASPL as seen in Figure 8. As much as these results are encouraging, the effect of the refraction is only slightly visible at a polar angle of 90° and not at all below. Therefore the good results can mainly be attributed to the correct estimation of the volume of sources able to propagate sound directly. The impact of the refraction will be seen more downstream.

As stated before, the comparison with the experiment is quite tricky above  $120^\circ$  because the noise level will be driven by the large scale turbulence. This can be seen in both Figure 11 and Figure 12. One can imagine two spectra, one that is present on all frequencies with a peak frequency of 500Hz and another that slowly grows in amplitude until overpassing the first one around  $120^\circ$ . This second spectrum is centered at a slightly lower frequency but is a lot narrower. This second spectrum is not predicted by this model.

The peak amplitude continues to grow but not as fast as the experiment because of the presence of the large scale turbulence. That behaviour was expected although the precision of the increase rate of the peak amplitude cannot be judged with this set of experiment. Nevertheless, one can also see that the peak frequency is clearly shifted back toward the lower frequencies matching in a better way the experiment. Because this local shift to the low frequencies gains in impact between  $90^\circ$  and  $105^\circ$  but slowly reincreases until reaching at  $135^\circ$  the same peak frequency as at  $75^\circ$ , it is clear that it is an effect of the refraction. This is explained by two facts. First, through the divergence and transmission coefficients, the ray with high incident refraction angles will be more attenuated than to the other rays. That means that sources located at an axial position close to the observer will be more defining in the frequential signature of the spectrum. Moreover, it is observed via the source model used presently that the sources responsible for the higher frequencies are located closer to the nozzle exit. It is a given that at polar angles around  $120^\circ$ , the observer axial position is quite downstream and therefore sources upstream will reach the observer with an incident refraction angle that is high. That means that the higher frequency sources will be highly attenuated by the different coefficients thus the refraction part is adding more energy to the total noise at lower frequency, inducing the shift of the peak frequency.

## 5. CONCLUSIONS

In this paper a methodology to introduce refraction effects in the Tam and Auriault model for fine scale jet mixing noise predictions using a two-part propagation technique is proposed. The path of the ray has been simplified to two segments with a sharp bend in the path instead of a progressive deviation through the mixing layer. The location of this bend has been explicitated through the building a 5-equation system. A Green function allowing the propagation through two different media has been proposed using as a starting point the convected Helmholtz equation's solution. This Green function has been verified to be equivalent to the classical formulation in the case of a continuous medium. Despite strong attenuations by both the transmission and the divergence factor, the

contribution of the refracted sources can be seen for an observer at a polar angle between  $90^\circ$  and  $135^\circ$  with a local increase of amplitude when integrating over the frequencies. The refraction part also induces a shift toward the lower frequencies of the peak of the PSD spectra. With the refraction part contribution slowly reducing and the direct part increasing, the cone of silence is highlighted with a plateau of the OASPL for polar angles above  $135^\circ$ .

## Acknowledgement

This work was performed within the framework of the Labex CeLyA of the Université de Lyon, within the programme 'Investissements d'Avenir' (ANR-10-LABX-0060/ANR-11-IDEX-0007) operated by the French National Research Agency (ANR). It was also performed with the valuable help of Jean-Yves Suratteau, Grégoire Pont and Jérôme Huber from Airbus.

## References

- [1] C. K. W. Tam, L. Auriault: Jet Mixing Noise from Fine-Scale Turbulence. *AIAA J.* 37 (1999) 145-153.
- [2] P. J. Morris, S. Boluriaan: The prediction of jet noise from CFD data. *AIAA Paper* 2004, 2004-2977.
- [3] S. A. E. Miller: Toward a comprehensive model of jet noise using an acoustic analogy. *AIAA J.* 52 (2014) 2143-2164.
- [4] C. K. W. Tam, M. Golebiowski, J. M. Steiner: On the two components of turbulent mixing noise from supersonic jets. *AIAA Paper* 1996, 1996-1716.
- [5] C. Bogey, O. Marsden: Simulations of initially highly disturbed jets with experiment-like exit boundary layers. *AIAA J.* 54 (2016) 1299-1312.
- [6] J. Huber, G. Drochon, C. Bonnaud, A. Pintado-Peno, F. Cléro, G. Bodard: Large-Scale Jet Noise Testing, Reduction and Methods Validation "EXEJET": 1. Project Overview and Focus on Installation. *AIAA Paper* 2014, 2014-3032.
- [7] P. O. A. L. Davies, M. J. Fisher, M. J. Barratt: The characteristics of the Turbulence in the Mixing Region of a Round Jet. *J. of Fluid Mech.*, Vol 15(3) (1963) 337-367.
- [8] S. Candel: Numerical solution of conservation equations arising in linear wave theory: Application to aeroacoustics. *J. of Fluid Mech.*, Vol 83(3) (1977), 465-493.
- [9] P. M. Morse, K. U. Ingard: *Theoretical Acoustics*. Princeton University Press, Princeton, New Jersey, 1968.
- [10] G. A. Deschamps: Ray Techniques in Electromagnetics. *Proc. IEEE* 60 (September 1972) 1022-1035.